



# Fabrication of micro–nano-roughened surface with superhydrophobic character on an aluminium alloy surface by a facile chemical etching process

MOHAMMAD REZA ATTAR<sup>1</sup>, EHSAN KHAJAVIAN<sup>1</sup>, SAMAN HOSSEINPOUR<sup>2,\*</sup>   
and ALI DAVOODI<sup>1</sup>

<sup>1</sup>Materials and Metallurgical Engineering Department, Faculty of Engineering, Ferdowsi University of Mashhad, Mashhad 91775-1111, Iran

<sup>2</sup>Institute of Particle Technology (LFG), Friedrich-Alexander-Universität-Erlangen-Nürnberg (FAU), Cauerstraße 4, 91058 Erlangen, Germany

\*Author for correspondence (saman.hosseinpour@fau.de)

MS received 27 April 2019; accepted 2 August 2019

**Abstract.** In the present work, we have fabricated a superhydrophobic surface on aluminium alloy 2024 through a simple immersion chemical etching method in hydrochloric acid followed by a functionalization step in stearic acid solution. The impact of etching time on water contact angle was investigated and a contact angle of  $\sim 167^\circ$  was reached on the superhydrophobic surface, which was etched for 4 min. Morphology of the surface was evaluated by scanning electron microscopy and the surface chemical analysis was performed by energy-dispersive X-ray spectroscopy and Raman spectroscopy. We show that the fabricated superhydrophobic samples can besides water, also repel other liquids. We also demonstrate the self-cleaning properties of the fabricated samples using graphite particles as contaminants. Ultimately, we assessed the corrosion resistance properties of the fabricated surfaces by the potentiodynamic polarization method. The superhydrophobic surface exhibited increased corrosion potential and polarization resistance along with reduced corrosion current density, all of which are indicative of a significant improvement in corrosion performance of the superhydrophobic surface in comparison with typical aluminium 2024. The cheap and facile superhydrophobic surface fabrication method presented in this study can be applied to large scale samples with no need for electricity or expensive raw materials.

**Keywords.** Superhydrophobic; aluminium alloy 2024; self-cleaning; corrosion.

## 1. Introduction

Superhydrophobic surfaces have recently attracted increased attention due to their unique water-repellent properties [1,2]. Such surfaces can be found in cell-repellent surfaces [3], low-adhesion surfaces [4], anti-icing surfaces [5,6] and self-cleaning surfaces [7], or in surfaces with reduced friction coefficient [8–10]. A superhydrophobic surface refers to a surface with water droplet contact angle greater than  $150^\circ$  and sliding angle less than  $10^\circ$  [11]. The superhydrophobicity phenomenon was first observed in nature in the lotus leaves [12,13] and since then several theories such as the Cassie–Baxter theory [14] have been presented to explain and justify this phenomenon. According to the Cassie–Baxter theory, the contact angle between the water droplet and the superhydrophobic surface depends on the roughness and the free energy of the surface. In a rough surface with low surface energy, air pockets will be trapped in cavities and grooves of the surface; thus a superhydrophobic surface can be obtained [15]. Various methods have been used so far for fabrication of superhydrophobic surfaces, including microwave-assisted chemical deposition methods [16], electrochemical methods

[17,18], chemical etching in acidic and basic solutions [19,20] and sol–gel method [21].

Aluminium and its alloys have been widely applied in numerous applications (e.g., in aerospace, marine, electrical and construction) owing to their unique physical and mechanical properties, abundance, low density, high thermal and electrical conductivity, high strength to weight ratio and high corrosion resistance [22]. Among aluminium alloys the 2000 series alloys are extensively employed in aerospace industry [23]. Nevertheless, their corrosion resistance is relatively weak among aluminium alloys. Therefore, the surfaces of 2000 series aluminium alloys are often modified to improve their corrosion resistance, among which increasing the hydrophobicity of surface is a very attractive method. Nevertheless, some of the aforementioned methods for fabrication of superhydrophobic surfaces are tedious, require electricity, expensive equipment and chemicals, and cannot be upscaled for industrial applications. In this study, we used a simple and cheap chemical etching method and surface functionalization on aluminium alloy 2024 to fabricate a superhydrophobic surface with improved corrosion resistance. The hydrophobicity of the surface was optimized by adjusting the chemical

etching time to provide the maximum corrosion resistance. We show that the fabricated superhydrophobic samples can besides water also repel other liquids with different properties. The self-cleaning properties of the fabricated superhydrophobic surfaces were demonstrated using graphite particles as contaminants. This method of fabricating superhydrophobic surfaces is inexpensive, and does not require advanced equipment and electricity, which paves the way for industrialization of superhydrophobic aluminium alloys.

## 2. Materials and methods

### 2.1 Materials

Aluminium 2024 alloy sheet with a thickness of 2 mm was used as a substrate. Hydrochloric acid, stearic acid, acetone, ethanol and deionized water were all used as received.

### 2.2 Fabrication of superhydrophobic surface

The aluminium alloy 2024 samples were cut into  $1.5 \times 1.5 \times 0.2 \text{ cm}^3$ , and were ground successively by #400, #800 and #1000 sandpapers. Samples were washed with distilled water and alcohol and dried in a stream of air. The samples were then chemically etched in an aqueous solution of hydrochloric acid (1:1 volume ratio) for different etching times. After washing with distilled water, the etched samples were immersed in a solution containing water and acetone (1:1 volume ratio) to remove the precipitates that remained from the etching step. Samples were then rinsed with distilled water and were functionalized by dipping in a 5 mM stearic acid in ethanol solution at room temperature for 1 h. Finally, the samples were dried at room temperature.

### 2.3 Characterization

A digital microscope (AnyWay, 500 $\times$ ) was used to capture the images of 4  $\mu\text{l}$  water droplets and the SolidWorks 2015 software was employed to calculate the droplet–surface contact angle. Surface morphology was observed by scanning electron microscopy (SEM) equipped with an energy-dispersive X-ray (EDX) analyser (SEM–EDX, PHENOM, Prox model) to determine the surface chemical composition. Raman spectroscopy was performed using a LabRam HR from Horiba with a 633 nm laser to confirm that the surface functionalization was performed successfully. In order to investigate the corrosion resistance of the samples, potentiodynamic polarization experiments were carried out in a corrosive solution of 60 mM NaCl at a potential scan rate of  $15 \text{ mV min}^{-1}$  (Potentiostat–Galvanostat model PG State 302 N from AutoLab). Pt electrode and saturated Calomel electrode (SCE) were used as the counter and reference electrodes, respectively.

## 3. Results

### 3.1 Surface morphology

The surface morphology of samples was investigated by SEM, as demonstrated in figure 1. Figure 1a shows the surface of the 2024 aluminium alloy after the polishing process. In this figure, the intermetallic particles (bright spots) protruding from the aluminium alloy surface and the lines created during polishing steps can be observed. Figure 1b presents the SEM image of the aluminium alloy after etching in hydrochloric acid for 4 min. As can be seen in this image, during the etching, the sample surface is roughened to a large extent. The sediments that are formed during the etching process are also observable in this image. These sediments are completely dissolved and removed in the washing step in acetone, as presented in figure 1c. Figure 1d shows the SEM image of the aluminium alloy surface after its immersion in stearic acid solution. No aggregates of stearic acid molecules are observed on the roughened aluminium surface, which shows that stearic acid is deposited as a thin and homogeneous layer. As it will be discussed later, adsorption of stearic acid on the roughened surface with micro- and nanostructures lowers the free energy of the surface, resulting in its superhydrophobicity [19,24].

### 3.2 Chemical composition of the surface

To determine the chemical composition of the aluminium alloy surface, before and after etching and functionalization, EDX analysis was performed and the results are depicted in figure 2. The quantitative elemental analyses of polished aluminium alloy and superhydrophobic aluminium alloy are presented in table 1. The EDX results clearly show that the chemical etching step has resulted in a change in the chemical composition of the aluminium surface, compared with that of the polished sample. Increased level of carbon is indicative of the adsorption of stearic acid molecules on the roughened surface [10,19]. Oxygen is also detected in the superhydrophobic sample due to the formation of metal oxide film on aluminium surface during the chemical etching step. Oxygen atom in the structure of adsorbed stearic acid also contributes to the oxygen peak in the EDX results. Figure 2c shows the Raman spectrum from the chemically etched and functionalized aluminium surface. The characteristic peaks of the stearic acid are clearly observed in this figure, confirming the adsorption of stearic acid molecules on the roughened surface. The assignment of the peaks in the Raman spectrum can be found in literature [25]. Based on the EDX analysis, the surface is covered with an oxide layer prior to the deposition of stearic acid. Therefore, the enhancement of the Raman signal due to surface plasmonic effects is plausible in this case, similar to previous surface-enhanced Raman scattering studies on aluminium surfaces [26].

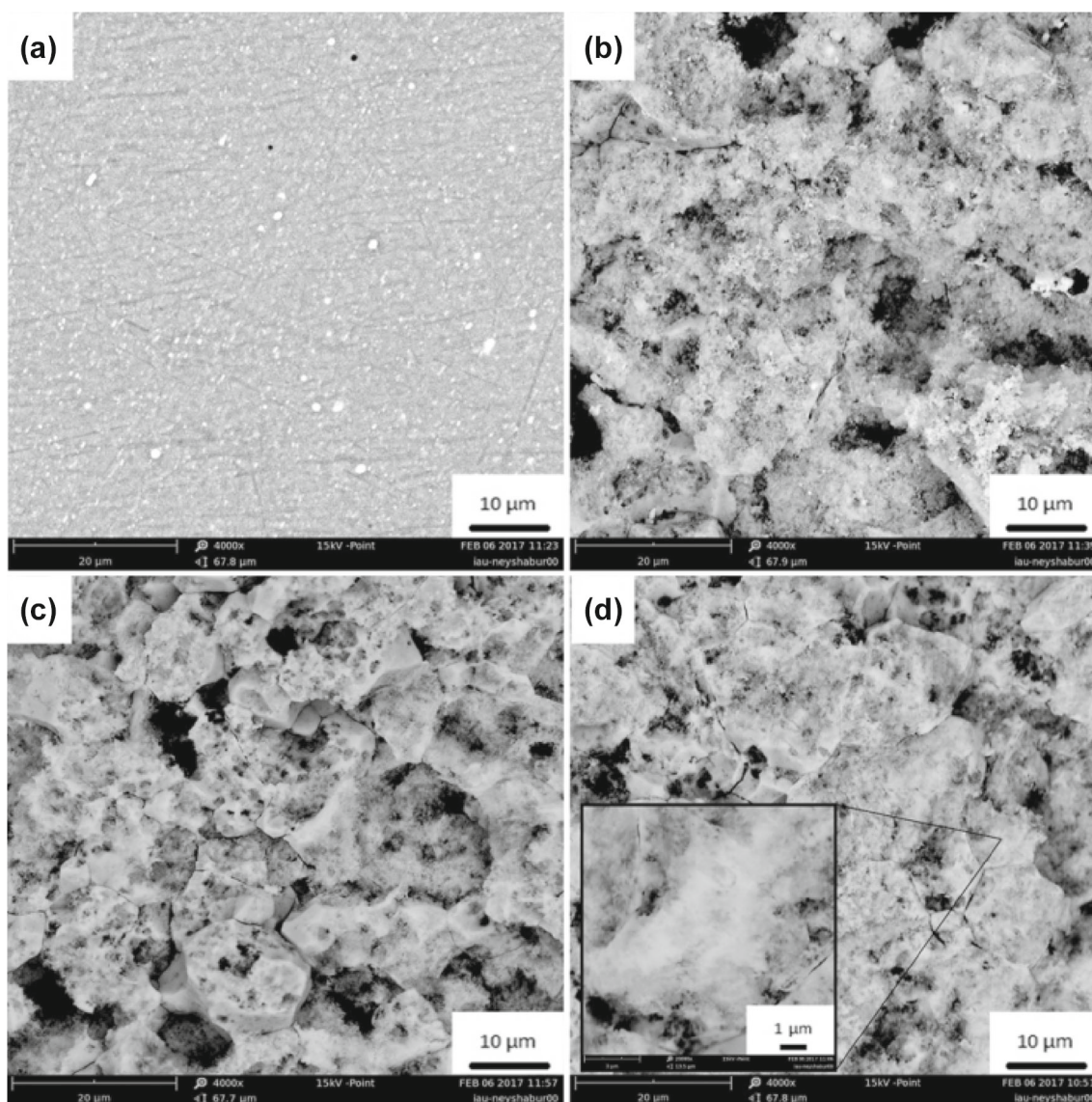


**Figure 1.** SEM images of the surface of: (a) as-polished, (b) HCl-etched, (c) acetone-cleaned and (d) stearic-acid-functionalized (superhydrophobic) 2024 aluminium alloy substrate.

### 3.3 Effect of etching time on contact angle

As discussed earlier, formation of a roughened surface (figure 1) and the successive deposition of low-surface-energy stearic acid will result in air entrapment between the surface of the superhydrophobic surface and water droplets, which prevents wetting of the surface. Roughness of the surface thus plays an important role in the superhydrophobic characteristics of surfaces. To achieve the optimum surface roughness that results in the highest superhydrophobicity, we functionalized samples that underwent chemical etching for different durations and investigated the effect of chemical etching time on the contact angle of the functionalized roughened surfaces. Figure 3 presents the effect of etching time on the wetting contact angle of the samples after 1 h

immersion in stearic acid solution. As can be seen, increasing the etching time from 1 to 4 min results in increased contact angle from  $\sim 84^\circ$  to  $\sim 167^\circ$ . The reason for improved contact angle of the functionalized surfaces by increased etching time is the increase in the surface roughness as the etching process is prolonged. In fact, chemical etching for less than 4 min does not result in complete and uniform roughening of the surface. Over-etching the sample for longer than 4 min did not further improve the superhydrophobicity of the surface and the contact angle remained unchanged. The surface–water droplet adhesion for the as-polished surface was high and the sliding angle exceeded  $80^\circ$ . However, after 4-min chemical etching and functionalization by stearic acid, the sliding angle reached very low values ( $\sim 3^\circ$ ).

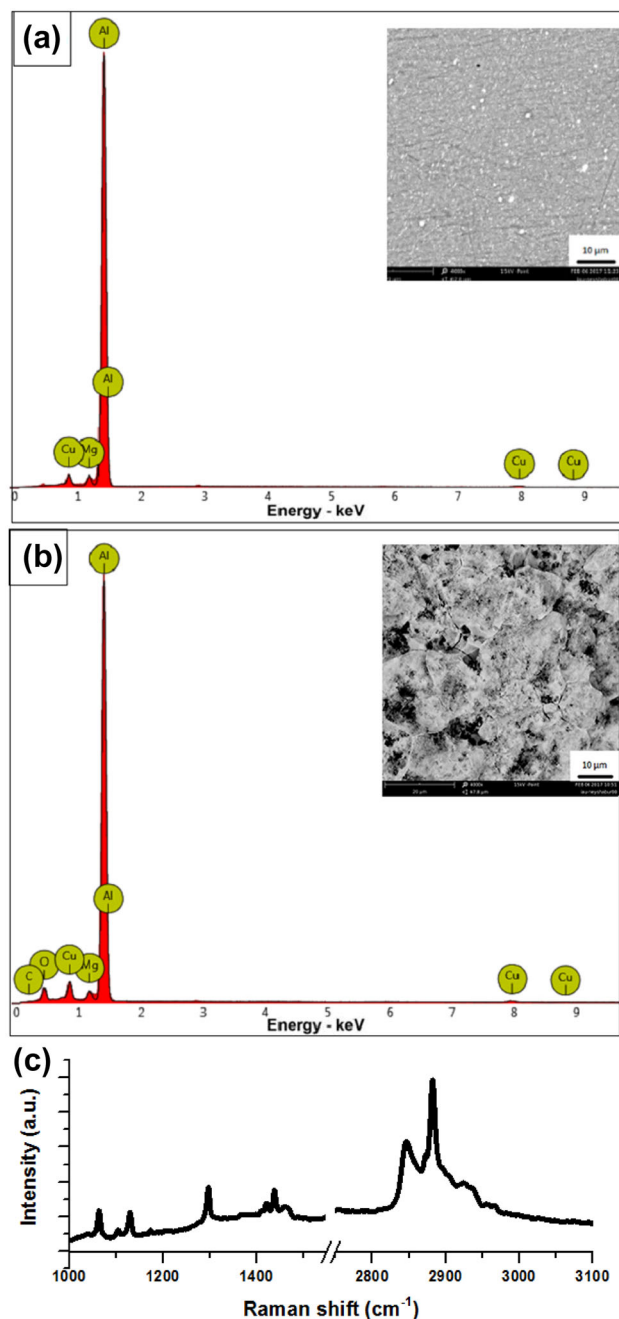


**Figure 2.** EDX spectra of: (a) as-polished and (b) etched and functionalized 2024 aluminium alloy samples. Insets show the SEM images of the area of which the EDX spectra are collected. (c) The Raman spectrum of the chemically etched aluminium surface after functionalization with stearic acid. Peak assignments can be found in literature [25].

### 3.4 Mechanism of superhydrophobic surface formation

Figure 4 illustrates the wetting behaviour of the water droplet on different surfaces. As shown in figure 4a, the water droplet on the surface of the polished 2024 aluminium alloy exhibits a wetting angle of  $80^\circ$ , consistent with the previous studies [27]. To measure the surface tension between the water droplet and the stearic acid, stearic acid powder (with melting point of  $60^\circ\text{C}$ ) was melted and then poured onto a flat glass surface. After solidification, the solid piece of stearic acid was turned over and contact angle of  $80^\circ$  was measured between water droplet and the flat stearic acid surface (figure 4b). The contact angle values on flat surfaces (presented in figure 4a and b) follow Young's equation [28]. Figure 4c presents a schematic image of a water droplet on a flat surface following Young's equation:

$$\gamma_{sv} = \gamma_{sl} + \gamma_{lv} \cos \theta \quad (1)$$

where  $\gamma_{sv}$  is the surface tension between the solid phase and air,  $\gamma_{sl}$  is the surface tension between the solid and liquid phases,  $\gamma_{lv}$  is the surface tension between the liquid phase and the air and  $\theta$  denotes the wetting contact angle. Considering the stearic acid–air surface tension ( $\gamma_{sv} = 27.7 \text{ dyn cm}^{-1}$ ) [29] and water–air surface tension ( $\gamma_{lv} = 78 \text{ dyn cm}^{-1}$ ) [30], the surface energy between stearic acid and water ( $\gamma_{sl}$ ) was calculated to be  $\sim 14.15 \text{ dyn cm}^{-1}$ . After chemical etching of the sample (which results in surface roughening) and its functionalization by stearic acid, the surface becomes superhydrophobic and its contact angle reaches  $\sim 167^\circ$  (figure 4d). As schematically illustrated in figure 4e, the superhydrophobic aluminium surface is composed of micron-size rough features covered by nanometric low-surface-energy stearic acid molecules. Consequently, air pockets can be entrapped at the water–solid interface, resulting in surface low contact angle. This superficial superhydrophobicity feature can be described in terms of the Cassie–Baxter theory [14]. Based on this theory, when the contact surface is composed of two different materials, Young's wettability equation can be rewritten as:

$$\cos \theta_{CA} = f \cos \theta + f - 1 \quad (2)$$

where  $\theta$  is the contact angle of the water droplet with the completely flat surface of the solid on the superhydrophobic surface (here the stearic acid). This value was previously measured to be  $80^\circ$ ;  $\theta_{CA}$  in equation (2) is the angle of water droplet on the superhydrophobic surface, which is measured to be  $\sim 167^\circ$  (figure 4d). In this equation,  $f$  is the ratio of entrapped

**Table 1.** EDX results of aluminium alloy 2024 before and after treatment.

Sample	Al (wt%)	O (wt%)	Cu (wt%)	Mg (wt%)	C (wt%)
As-polished Al alloy	94.1	0.1	3.7	2.1	—
Superhydrophobic Al alloy	79.1	9.4	4.9	1.7	4.9

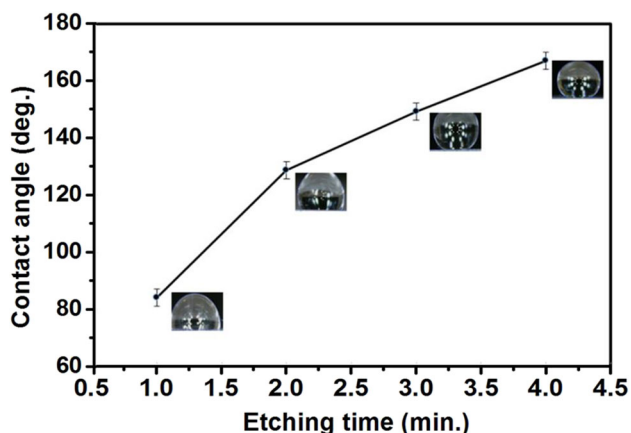


**Figure 3.** Water droplet contact angle of functionalized aluminium surfaces after different chemical etching durations.

air at the superhydrophobic surface to the total liquid-exposed surface. By replacing the mentioned values in equation (2), this ratio can be calculated ( $f = 0.97$ ). This means that 97% of the water-droplet-exposed superhydrophobic surface is composed of air and the rest is the nano-precipitants of stearic acid molecules deposited on the micro-roughness

of the aluminium alloy, which is consistent with previous studies [31]. As inferred from the Cassie–Baxter theory, besides surface roughness, presence of substances of low surface free energy plays a crucial role in surface superhydrophobicity. Stearic acid has been previously shown to adsorb on metallic surfaces for improved corrosion resistance [32]. Apart from stearic acid, which has been used in this study, other organic molecules and fatty acids with different aliphatic chain lengths have also been used to lower the surface free energy of the micro–nano-structured substrates [27,33,34], which result in the formation of superhydrophobic surfaces. Besides static contact angle, sliding angle is also an important parameter in characterizing a superhydrophobic surface. In some cases, in spite of high contact angle, the water droplet may adhere to the surface and may not easily slide, which is not a desirable property for some applications such as self-cleaning [35]. Nevertheless, our measurements in the present study show that the 2024 aluminium alloy chemically etched for 4 min and functionalized exhibits, besides its very high static contact angle, a very low sliding angle of  $\sim 3^\circ$ . This very low sliding angle makes the presented surface modification method a good candidate for fabrication of surfaces with self-cleaning properties, as will be discussed in the following sections.

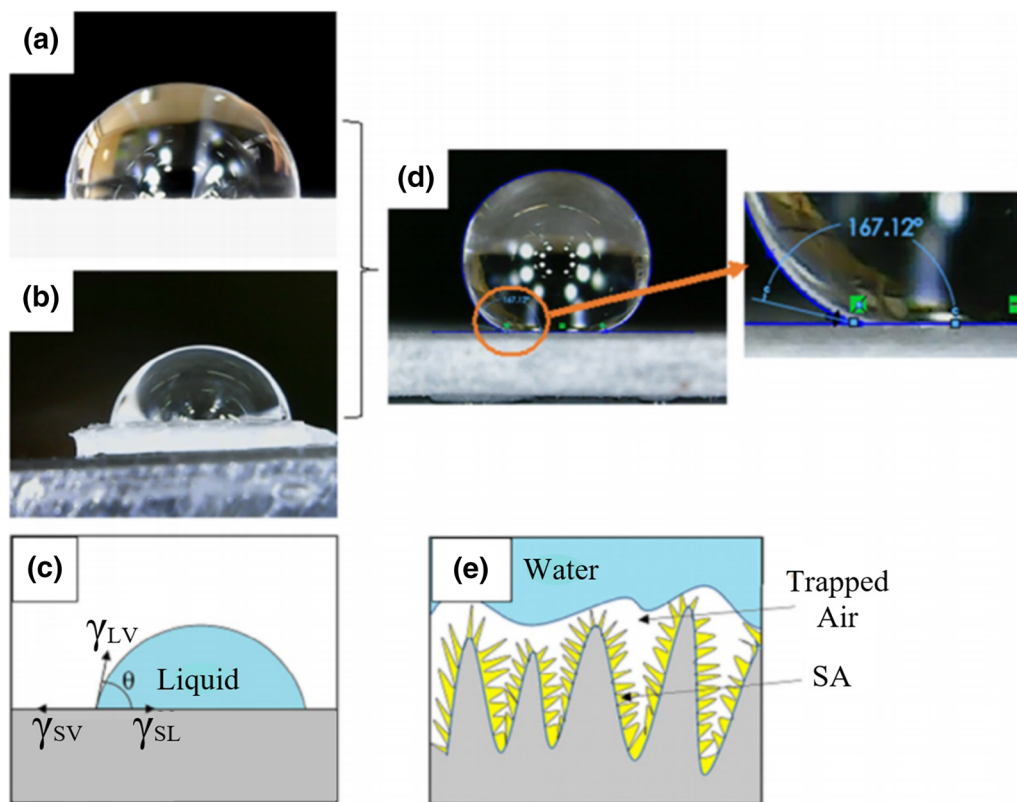


**Figure 4.** Drops of water on (a) as-polished aluminium surface and (b) a piece of molten and re-solidified stearic acid. (c) Schematic illustration of a water droplet on a flat surface. (d) Water contact angle on 4-min-etched sample after functionalization by stearic acid alongside the enlarged droplet–aluminium interface image. (e) Schematic illustration of water droplet on a roughened superhydrophobic surface.

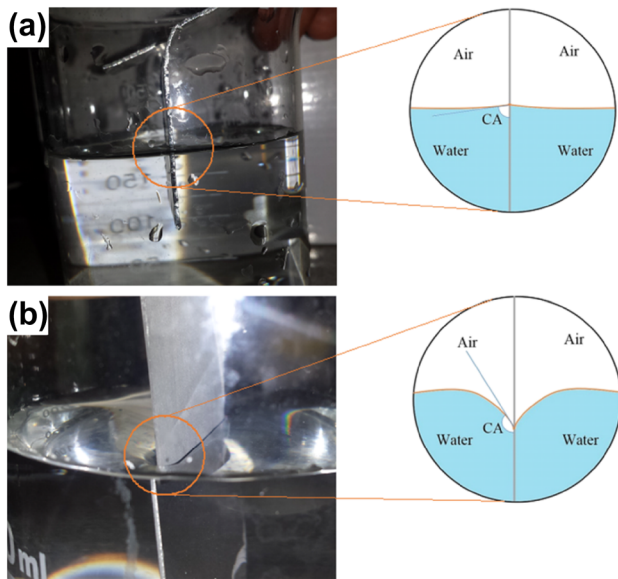


**Figure 5.** Illustration of the wettability of: (a) the as-polished aluminium and (b) the chemically etched and functionalized superhydrophobic aluminium alloy. Corresponding liquid–solid–air interface is also schematically presented.

### 3.5 Immersion in water

Another illustration for the superhydrophobicity of the chemically etched and functionalized aluminium surface can be observed in figure 5a and b. In this figure, optical images at solid–liquid interface for as-polished and superhydrophobic aluminium samples are presented, clearly demonstrating the effect of surface treatment on the wettability of the surface. The corresponding liquid–solid–air interface is also schematically presented in this figure. When the aluminium surface is inserted into water, an angle of  $\sim 90^\circ$  forms between water and as-polished aluminium (figure 5a), and water wets the surface with an almost flat boundary. Chemical etching and surface functionalization result in a convex boundary between water and solid surface, which preserves the surface from wetting. As discussed earlier, entrapment of air gaps between water and low-energy surface in the superhydrophobic surface is responsible for this observation.

### 3.6 Self-cleaning behaviour

As discussed earlier, the small rolling angle of water droplet in superhydrophobic surfaces allows them to be used in the

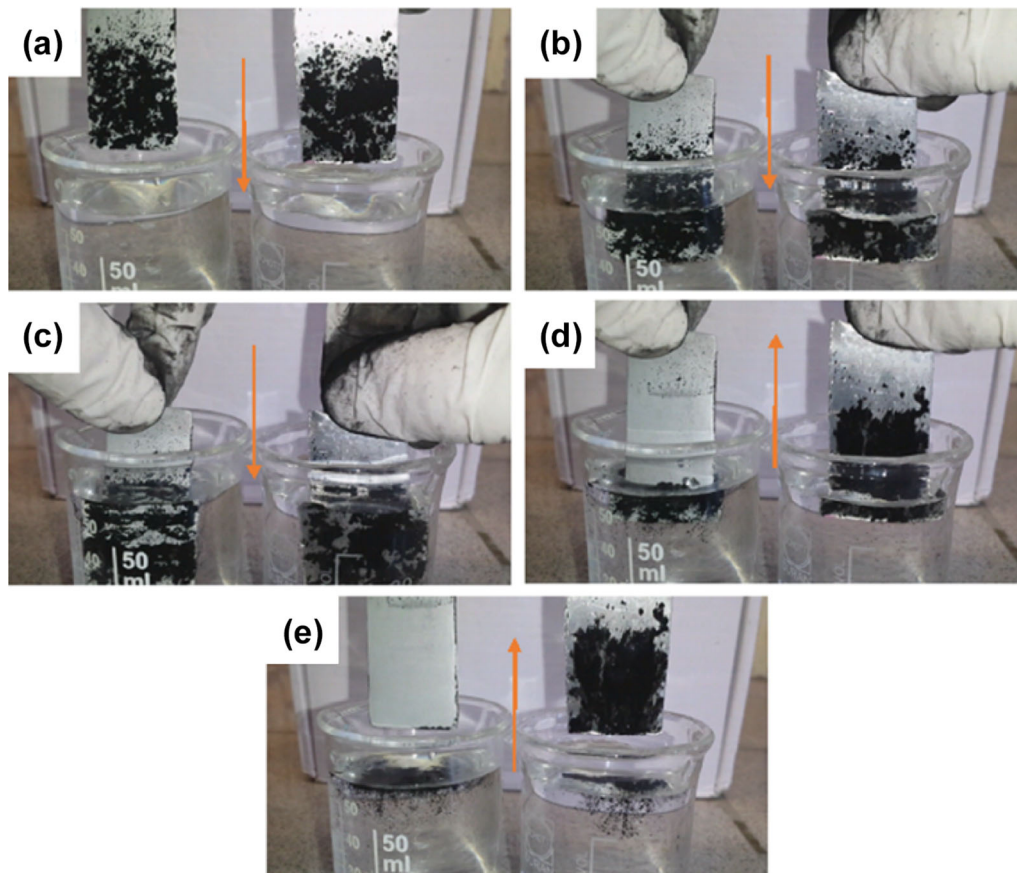


**Figure 6.** Self-cleaning ability of the immersion-etched Al–STA superhydrophobic aluminium alloy surface: (a)–(c) dipping and (d)–(e) rising steps.

self-cleaning applications. Figure 6 demonstrates the self-cleaning behaviour of a superhydrophobic aluminium alloy compared with as-polished sample. For the purpose of demonstration, some graphite powder, as contaminant, was poured on the surface of both samples and the specimens were dipped in water as shown in figure 6a–c. Figure 6d and e

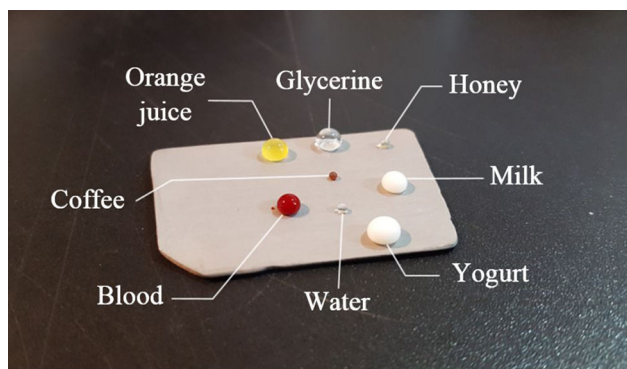


**Figure 7.** Demonstration of surface repellence for droplets of different liquids: water, yogurt, milk, honey, glycerine, orange juice, coffee and blood on the fabricated superhydrophobic 2024 aluminium alloy surface.

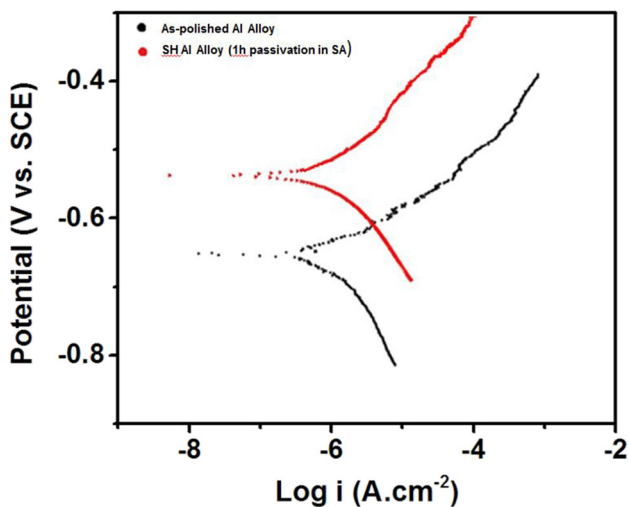


**Figure 8.** Potentiodynamic polarization curves of the as-polished and fabricated superhydrophobic aluminium alloy surfaces in 60 mM aqueous sodium chloride solution.

display the samples when they are removed from the water. As is clear from these pictures, during samples removal from water, the graphite particles still adhere to the as-polished aluminium sample. In contrast, the graphite particles are completely removed from the superhydrophobic sample during its removal from water. Considering the fact that graphite is a hydrophobic substance, its complete removal from the fabricated superhydrophobic surface is a direct demonstration of the effectiveness of this surface treatment for fabrication of self-cleaning surfaces.

To further explore the self-cleaning properties of the fabricated superhydrophobic surface, droplets of different liquids with various hydrophobicities and viscosities were placed on the surface of the superhydrophobic 2024 aluminium alloy. Figure 7 visualizes how eight different liquid droplets, including glycerine, honey, yogurt, milk, coffee, orange juice and blood, do not wet the surface of the superhydrophobic aluminium alloy.

### 3.7 Corrosion behaviour

One of the most desirable properties of superhydrophobic surfaces is their anti-corrosion properties. In superhydrophobic surfaces, due to the formation of an air mediator layer between the liquid and surface [5,8], a smaller area of the surface is exposed to the corrosive environment, which in turn results in an increase in the surface resistance to corrosion. To assess the effectiveness of our fabrication method in improving the corrosion resistance of the 2024 aluminium alloy, we performed potentiodynamic polarization measurements on as-polished and superhydrophobic samples in 60 mM sodium chloride solution (figure 8). Tafel extrapolation was used to extract quantitative data from the potentiodynamic polarization measurements and the results are tabulated in table 2. As shown in this table, the corrosion current density of the as-polished aluminium sample is  $1.4 \mu\text{A cm}^{-2}$ . After chemical etching for 4 min and functionalization in stearic acid, the corrosion current density was reduced to  $0.7 \mu\text{A cm}^{-2}$ . The corrosion potential of the as-polished aluminium alloy ( $-643 \text{ mV vs. SCE}$ ) was also enhanced after it was converted to a superhydrophobic surface ( $-528 \text{ mV vs. SCE}$ ). The polarization resistance of as-polished aluminium surface was calculated as  $20.2 \text{ k}\Omega \text{ cm}^2$ . After etching for 4 min and functionalization with stearic acid, the surface polarization resistance augmented to  $36.1 \text{ k}\Omega \text{ cm}^2$ . Our electrochemical measurements confirm that the fabricated superhydrophobic

**Table 2.** Parameters extracted from Tafel extrapolation on polarization plots in figure 8 for as-polished and superhydrophobic 2024 aluminium alloy. Potentials are reported against SCE.

Sample	Anodic slope ( $\text{mV dec}^{-1}$ )	Cathodic slope ( $\text{mV dec}^{-1}$ )	$V_{\text{CORR}}$ (mV)	$i_{\text{CORR}}$ ( $\mu\text{A cm}^{-2}$ )	$R_P$ ( $\text{k}\Omega \text{ cm}^2$ )
As-polished	177	66	$-643 \pm 15$	$1.4 \pm 0.05$	$20.2 \pm 0.5$
Superhydrophobic	112	111	$-528 \pm 10$	$0.7 \pm 0.08$	$36.1 \pm 0.8$

sample exhibits superior corrosion resistance compared with its as-polished counterpart.

#### 4. Conclusion

In this work, a facile and very low-cost chemical etching method followed by a functionalization step in stearic acid was employed to achieve superhydrophobic surface on aluminium alloy 2024. The effect of the etching time on the superhydrophobicity of the samples was studied and water contact angle of  $\sim 167^\circ$  was achieved for samples etched for optimum duration of 4 min. The deposition of nano-scale low-surface-energy stearic acid molecules on micron range rough samples is responsible for the superhydrophobicity of the fabricated surfaces. The main mechanism of superhydrophobicity is the entrapped air pockets in the rough structure of the surface, which comprise 97% of the water droplet-exposed area of the superhydrophobic surface. The potentiodynamic polarization measurements show that the corrosion resistance of the superhydrophobic surface is significantly improved compared with as-polished 2024 aluminium alloy. The self-cleaning properties of the superhydrophobic surface were demonstrated using graphite particles as contaminant and it was also shown that the fabricated surface is capable of repelling most of the liquids. This fabrication method does not require expensive chemicals, sophisticated equipment or electricity; therefore, it is suitable for upscaling and for application in industries.

#### Acknowledgements

MRA, EK and AD thank Ferdowsi University of Mashhad, Iran, for providing laboratory facilities. SH thanks Prof W Peukert and Emerging Talents Initiative (ETI) 2018/2\_Tech\_06, FAU (Grant No. 2018/2), Germany, grant for supporting his research.

#### References

- [1] Ramachandran R, Sobolev K and Nosonovsky M 2015 *Langmuir* **31** 1437
- [2] Lu Y, Sathasivam S, Song J, Crick C R, Carmalt C J and Parkin I P 2015 *Science* **347** 1132
- [3] Stancu E C, Ionita M D, Vizireanu S, Stanciuc A M, Moldovan L and Dinescu G 2010 *Mater. Sci. Eng. B* **169** 119
- [4] Honeychuck R V, Ho T, Wynne K J and Nissan R A 1993 *Chem. Mater.* **5** 1299
- [5] Sarkar D K and Farzaneh M 2009 *J. Adhes. Sci. Technol.* **23** 1215
- [6] Farhadi S, Farzaneh M and Kulinich S A 2011 *Appl. Surf. Sci.* **257** 6264.
- [7] Bhushan B, Jung Y C and Koch K 2009 *Langmuir* **25** 3240
- [8] Dong H, Cheng M, Zhang Y, Wei H and Shi F 2013 *J. Mater. Chem.* **1** 5886
- [9] McHale G, Flynn M R and Newton M I 2011 *Soft Matter* **7** 10100
- [10] Li P, Chen X, Yang G, Yu L and Zhang P 2014 *Appl. Surf. Sci.* **300** 184
- [11] Li M, Zhai J, Liu H, Song Y, Jiang L and Zhu D 2003 *J. Phys. Chem. B* **107** 9954
- [12] Zhang X, Shi F, Niu J, Jiang Y and Wang Z 2008 *J. Mater. Chem.* **18** 621
- [13] Barthlott W and Neinhuis C 1997 *Planta* **202** 1
- [14] Cassie A B D and Baxter S 1944 *Trans. Faraday Soc.* **40** 546
- [15] Bittoun E and Marmur A 2009 *J. Adhes. Sci. Technol.* **23** 401
- [16] Liu Y, Tan T, Wang B, Zhai R, Song X, Li E *et al* 2008 *J. Colloid Interf. Sci.* **320** 540
- [17] Huang Y, Sarkar D K and Chen X G 2015 *Appl. Surf. Sci.* **327** 327
- [18] Xu N, Sarkar D K, Chen X G and Tong W P 2016 *Surf. Coat. Technol.* **302** 173
- [19] Ruan M, Li W, Wang B, Luo Q, Ma F and Yu Z 2012 *Appl. Surf. Sci.* **258** 7031
- [20] Saleema N, Sarkar D K, Paynter R W and Chen X G 2010 *ACS Appl. Mater. Interfaces* **2** 2500
- [21] Li Q, Yan Y, Yu M, Song B, Shi S and Gong Y 2016 *Appl. Surf. Sci.* **367** 101
- [22] Song-Mei L, Bin L, Jian-Hua L and Mei Y 2012 *Chin. J. Inorg. Chem.* **28** 1755
- [23] Zhao J, Xia L, Sehgal A, Lu D, McCreery R L and Frankel G S 2001 *Surf. Coat. Technol.* **140** 51
- [24] Hosono E, Fujihara S, Honma I and Zhou H 2005 *J. Am. Chem. Soc.* **127** 13458
- [25] Thompson W R and Pemberton J E 1995 *Langmuir* **11** 1720
- [26] Mogensen K B, Gühlke M, Kneipp J, Kadkhodazadeh S, Wagner J B, Espina Palanco M *et al* 2014 *Chem. Commun.* **50** 3744
- [27] Huang Y, Sarkar D K and Grant Chen X 2015 *Appl. Surf. Sci.* **356** 1012
- [28] Young T 1805 *Philos. Trans. R Soc. Lond.* **95** 65
- [29] Gros A T and Feuge R O 1952 *J. Am. Oil Chem. Soc.* **29** 313
- [30] Vargaftik N B, Volkov B N and Voljak L D 1983 *J. Phys. Chem. Ref. Data* **12** 817
- [31] Wu R, Liang S, Pan A, Yuan Z, Tang Y, Tan X *et al* 2012 *Appl. Surf. Sci.* **258** 5933
- [32] Gretić Z H, Mioč E K, Čadež V, Šegota S, Otmačić Ćurković H and Hosseinpour S 2016 *J. Electrochem. Soc.* **163** C937
- [33] Zheng S, Li C, Fu Q, Hu W, Xiang T, Wang Q *et al* 2016 *Mater. Des.* **93** 261
- [34] Noorbakhsh Nezhad A H, Arefinia R, Kashefi M, Davoodi A and Hosseinpour S 2019 *Appl. Surf. Sci.* **493** 1243
- [35] Li H J, Fan W Z, Pan H H, Wang C W, Qian J and Zhao Q Z 2017 *Chem. Phys. Lett.* **667** 20